MOLECULAR PHYSICS, 2015
http://dx.doi.org/10.1080/00268976.2015.1126367

Taylor & Francis
Taylor & Francis Group

55TH SANIBEL SYMPOSIUM - SPECIAL ISSUE

New massively parallel linear-response coupled-cluster module in ACES III: application to static polarisabilities of closed-shell molecules and oligomers and of open-shell radicals

Prakash Verma[a,1], Ajith Perera[a,b] and Jorge A. Morales[a]

[a]Department of Chemistry and Biochemistry, Texas Tech University, Lubbock, TX, USA; [b]Department of Chemistry, Quantum Theory Project, University of Florida, Gainesville, FL, USA

ABSTRACT

Stemming from our implementation of parallel coupled-cluster (CC) capabilities for electron spin resonance properties [J. Chem. Phys. **139**, 174103 (2013)], we present a new massively parallel linear response CC module within ACES III. Unlike alternative parallel CC modules, this general purpose module evaluates any type of first- and second-order CC properties of both closed- and open-shell molecules employing restricted, unrestricted and restricted-open-shell Hartree–Fock (HF) references. We demonstrate the accuracy and usefulness of this module through the calculation of static polarisabilities of large molecules. Closed-shell calculations are performed at the following levels: second-order many-body perturbation theory [MBPT(2)], CC with single- and double-excitations (CCSD), coupled-perturbed HF and density functional theory (DFT), and open-shell calculations at the unrestricted CCSD (UCSSD) one. Applications involve eight closed-shell organic-chemistry molecules (Set I), the first four members of the closed-shell thiophene oligomer series (Set II), and five open-shell radicals (Set III). In Set I, all calculated average polarisabilities agree reasonably well with experimental data. In Set II, all calculated average polarisabilities vs. the number of monomers show comparable values and saturation patterns and demonstrate that experimental polarisabilities may be inaccurate. In Set III, UCCSD perpendicular polarisabilities show a reasonable agreement with previous UCCSD(T) and restricted-open-shell-MBPT(2) values.

$$\alpha_{ij} = \left.\frac{\partial^2 \Delta E_{CC}}{\partial F_i F_j}\right|_{F=0} = \left\langle \Phi_0 \left| \hat{\Lambda}^{F_j} \bar{\hat{H}}_i^{(F)} \right| \Phi_0 \right\rangle + \left\langle \Phi_0 \left| \left(1+\hat{\Lambda}\right) \left[\bar{\hat{H}}_i^{(F)}, \hat{T}^{F_i} \right] \right| \Phi_0 \right\rangle$$

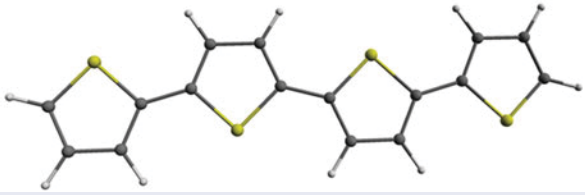

ARTICLE HISTORY
Received 4 November 2015
Accepted 24 November 2015

KEYWORDS
Coupled-cluster theory; coupled-cluster response treatment of properties; massively parallel coupled-cluster implementations to evaluate properties; static dipole polarisabilities

1. Introduction

The calculation of molecular properties with predictive accuracy is one of the most important endeavours in quantum chemistry. Quantitative molecular properties targeted for prediction pertain to almost all areas of chemistry and include geometry structures, linear and non-linear optical properties, excitation and ionisation energies, electron affinities, nuclear magnetic resonance (NMR) parameters and electron spin resonance (ESR) quantities, *inter alia* [1–5]. Various calculation factors affect the accuracy of the predicted properties (e.g. basis sets, vibrational, environmental and relativistic effects); however, for many properties, the inclusion of high levels of electron correlation effects is the decisive factor for their accuracy. Therefore, to calculate properties of large molecules, Kohn–Sham density functional theory (KS DFT) [6,7] is usually favoured over wavefunction-based alternatives [3,8] due to its attainment of electron correlation effects at low computation cost. While many of its properties are correct, KS DFT failures with

CONTACT Jorge A. Morales jorge.morales@ttu.edu
[1]Present Address: Department of Chemistry, Emory University, Atlanta, Georgia 30322, USA.

properties' predictions are well-known and documented [8–11]; these failures stem from inherent deficiencies in KS DFT [12–16] such as the self-interaction [17–19] and delocalisation [20] errors, *inter alia*. For instance, pertinent to the properties herein considered, Kirtman, Champagne *et al.* [9–11] have shown that KS DFT usually overestimates the (hyper)polarisability values of polymers due to an incorrect electric-field dependence in the response part of many exchange-correlation potentials [9]. In contrast, wavefunction-based methods, including the simplest Hartree–Fock (HF) method, do not exhibit these (hyper)polarisabilities' overestimations because they do not involve KS DFT exchange-correlation functionals (cf. Section 4).

Unlike KS DFT, wavefunction-based post-HF methods [2,21] [e.g. many-body perturbation theory (MBPT), coupled-cluster (CC) theory, configuration interaction and multi-reference approaches] are computationally expensive but provide properties with accurate and controllable predictability, free of the aforesaid KS DFT deficiencies. Certainly, the CC methods [2,22–24] do not escape from this situation because, except for their finite-order approximations [e.g. second-order MBPT [MBPT(2)] [25,26] and linear CC [27,28]], they exhibit an exacting trade-off between high accuracy and computational cost. For instance, the CC with single, double and perturbative triple excitations [CCSD(T)] [29,30] method is recognised as the 'gold standard' for electronic structure calculations, but it is nonetheless computationally onerous.

To overcome the discussed limitations, leading quantum chemistry codes such as CFOUR [31], GAMESS [32–34], Gaussian [35], Molpro [36,37], NWChem [38], ORCA [39] and Q-Chem [40] include some form of parallel CC capabilities to expedite CC applications. Moreover, the codes ACES III [41], NWChem [38] and PSQ [42] offer a higher class of CC parallel implementations designed to perform effectively on the massively parallel scale. Noteworthy, the parallel CC capabilities in ACES III [41] and NWChem [38] are not restricted to routine ground-state energy calculations but extend to linear-response properties calculations. In fact, NWChem [38] featured the first massively parallel linear-response CC implementation to calculate polarisabilities. Thus, with those resources, Hammond *et al.* [43] calculated the dynamic polarisabilities of large polyaromatic hydrocarbons (pyrene and the oligoacene series from benzene to hexacene) with the CC with single- and double-excitations (CCSD) method, and Kowalski *et al.* [44] calculated the static and dynamic polarisabilities of the C_{60} fullerene with the CCSD method for the first time. The latter study documents C_{60} as the largest molecule in absolute terms treated for CCSD polarisability calculations to date [44].

The massively parallel code ACES III [41] is characterised by its utilisation of various state-of-the-art advancements for parallel programming. These include the Super Instruction Processor (SIP) [45] and the Super Instruction Architecture Language (SIAL) [46] to execute and develop parallel codes, respectively, and the parallel OED/ERD atomic integral package [47]; the latter is one of the fastest packages to evaluate atomic integrals. Remarkably, ACES III's parallel tools were developed in house, independently from previous efforts, and, therefore, differ from the parallel tools in the NWChem's Global array toolkit. Originally, ACES III's parallel CC capabilities were limited to the calculation of primary properties (e.g. ground- and excited-state energies, molecular geometries, vibration frequencies, etc.) [41]. However, to enhance those capabilities, we have implemented a massively parallel general-purpose linear-response CC (LR-CC) module [48] in ACES III to evaluate any type of properties from first to second order (i.e. from zero- to linear-response regime). Furthermore, this module is not limited to property calculations with closed-shell molecules as is the case with its NWChem counterpart to the best of our knowledge. This last aspect reflects our primary interest in evaluating ESR properties [48], which are only relevant to open-shell molecules. A previously published article on ESR isotropic hyperfine coupling constants $A_{iso,N}$ [48] of large radicals illustrated our open-shell CC first-order property implementations, and the forthcoming articles on the ESR **g**- and **D**-tensors [49] will illustrate our open-shell CC second-order (linear-response) implementations. However, for second-order properties, the LR-CC module's capabilities can be more easily illustrated with the calculation of static dipole polarisabilities [50–52] – an important type of second-order property that is computationally less demanding to evaluate than the ESR **g**- and **D**-tensors. For these reasons, we report herein the theoretical foundations, performance and application of this massively parallel LR-CC module through the calculation of static polarisabilities of large molecules at the MBPT(2) and CCSD levels. Besides, the implementation of this parallel LR-CC module and its application to polarisabilities are complementary to previous NWChem efforts [43,44]. Before concluding, it should be emphasised that aside from reporting a milestone in our development of massively parallel CC capabilities [48], the calculated polarisabilities are valuable by themselves given the relevance of this property in chemistry, physics, materials science and technology [50–52]. This relevance is attested by the numerous

theoretical studies devoted to predict accurate polarisabilities [9–11,43,44,53–60].

This article is organised as follows. In Section 2, we summarise the theory on the CC response treatment of properties that is the foundation of the massively parallel LR-CC module in ACES III [41]. In Section 3, we present the computational details of this study and a performance analysis of the developed module. In Section 4, we present and discuss the calculated static polarisabilities and related properties at the coupled-perturbed HF (CPHF), DFT, MBPT(2) and CCSD levels in comparison with available experimental data. Finally, in Section 5, we present the main conclusions from this study.

2. Theory

The CC response treatment of properties is explained in detail in Refs. [61–65] and references cited therein. Therefore, here, we present a brief review of its theory as is employed for the present efforts. The CC response treatment of properties [61–65] starts with a perturbed Hamiltonian $\hat{H}$:

$$\hat{H}(\boldsymbol{\lambda},\boldsymbol{\mu}) = \hat{H}_0 + \sum_{i=1}^{N_\lambda} \lambda_i \hat{H}_i^{(\lambda)} + \sum_{i=1}^{N_\mu} \mu_i \hat{H}_i^{(\mu)} + \sum_{i,j=1}^{N_\lambda,N_\mu} \lambda_i \mu_j \hat{H}_{ij}^{(\lambda\mu)} \quad (1)$$

that is partitioned into an unperturbed, zeroth-order, Hamiltonian $\hat{H}_0$ and into first-order, $\sum_{i=1}^{N_\lambda} \lambda_i \hat{H}_i^{(\lambda)}$ and $\sum_{i=1}^{N_\lambda} \mu_i \hat{H}_i^{(\mu)}$, and second-order, $\sum_{i,j=1}^{N_\lambda,N_\mu} \lambda_i \mu_j \hat{H}_{ij}^{(\lambda\mu)}$, perturbation terms with respect to the strength parameters $\boldsymbol{\lambda} = (\lambda_1, \lambda_2, \ldots \lambda_{N_\lambda})$ and $\boldsymbol{\mu} = (\mu_1, \mu_2, \ldots \mu_{N_\mu})$. Properties of our immediate interest (e.g. dipole polarisability and ESR tensors [48,49]) can be evaluated with the Hamiltonian $\hat{H}(\boldsymbol{\lambda},\boldsymbol{\mu})$ in Equation (1). The specific identities of the perturbation terms and strength parameters in $\hat{H}(\boldsymbol{\lambda},\boldsymbol{\mu})$ depend on the particular property being calculated as shown at the end of this section.

In the CC theory [2,22,23], the exact wavefunction $|\Psi\rangle_{CC}$ of a molecule is $|\Psi\rangle_{CC} = \exp(+\hat{T})\,|\Phi_0\rangle$, where $|\Phi_0\rangle$ is an HF reference wavefunction and $\hat{T} = \hat{T}_1 + \hat{T}_2 + \cdots \hat{T}_n + \cdots$ is the excitation operator in terms of single-, $\hat{T}_1$, double-, $\hat{T}_2$, … and n-excitation, $\hat{T}_n$, operators from $|\Phi_0\rangle$. Denoting occupied and virtual HF spin-orbitals with the indices: $i, j, \ldots$ etc., and $a, b, \ldots$ etc., respectively, then, $|\Phi_0\rangle = |i, j, \ldots\rangle$ and $\hat{T}_n = (n!)^{-2} \sum_{ij\ldots}^{ab\ldots} t_{ij\ldots}^{ab\ldots} \{\hat{a}^\dagger \hat{i} \hat{b}^\dagger \hat{j} \ldots\}$, where $\hat{i}, \hat{j}\ldots$ etc. $\hat{a}^\dagger, \hat{b}^\dagger \ldots$ etc. are the spin-orbitals' annihilation and creation operators, respectively, $t_{ij\ldots}^{ab\ldots}$ … etc. are the CC excitation amplitudes, and $\{\ldots\}$denotes normal order. The CC energy functional $\Delta E_{CC}(\boldsymbol{\lambda},\boldsymbol{\mu})$ from the perturbed Hamiltonian $\hat{H}(\boldsymbol{\lambda},\boldsymbol{\mu})$ is [66–69] (cf. also Ref. [22])

$$\Delta E_{CC}(\boldsymbol{\lambda},\boldsymbol{\mu}) = \langle\Phi_0|\,(1+\hat{\Lambda})\bar{\hat{H}}(\boldsymbol{\lambda},\boldsymbol{\mu})\,|\Phi_0\rangle \quad (2)$$

where Δ denotes correlation correction, $\bar{\hat{H}}(\boldsymbol{\lambda},\boldsymbol{\mu}) = \exp(-\hat{T})\hat{H}(\boldsymbol{\lambda},\boldsymbol{\mu})\exp(+\hat{T})$is the similarity-transformed Hamiltonian and $\hat{\Lambda}$ the CC de-excitation operator. Like $\hat{T}$, $\hat{\Lambda}$ is expressed as $\hat{\Lambda} = \hat{\Lambda}_1 + \hat{\Lambda}_2 + \cdots \hat{\Lambda}_n + \cdots$, where $\hat{\Lambda}_1, \hat{\Lambda}_2, \ldots \hat{\Lambda}_n$ are single-, double-, … n-de-excitation operators: $\hat{\Lambda}_n = (n!)^{-2} \sum_{ij\ldots}^{ab\ldots} \tilde{\lambda}_{ij\ldots}^{ab\ldots} \{\hat{i}^\dagger \hat{a} \hat{j}^\dagger \hat{b} \ldots\}$, with CC de-excitation amplitudes $\tilde{\lambda}_{ij\ldots}^{ab\ldots}$. $\Delta E_{CC}(\boldsymbol{\lambda},\boldsymbol{\mu})$ satisfies a generalised Hellmann–Feynman theorem [67] and, therefore, it is conveniently adopted for properties' calculations resulting from its derivatives with respect to the strength parameters. Full determination of $|\Psi\rangle_{CC}$ and $\Delta E_{CC}(\boldsymbol{\lambda},\boldsymbol{\mu})$ requires the knowledge of the CC amplitudes $t_{ij\ldots}^{ab\ldots}$ and $\tilde{\lambda}_{ij\ldots}^{ab\ldots}$; these are obtained through the stationary conditions $\partial\Delta E_{CC}(\boldsymbol{\lambda},\boldsymbol{\mu})/\partial t_{ij\ldots}^{ab\ldots} = 0$ and $\partial\Delta E_{CC}(\boldsymbol{\lambda},\boldsymbol{\mu})/\partial\tilde{\lambda}_{ij\ldots}^{ab\ldots} = 0$ that lead to the $\hat{T}$- and $\hat{\Lambda}$-equations, Equations (3) and (4), respectively [2,22,23]

$$\hat{Q}\bar{\hat{H}}(\boldsymbol{\lambda},\boldsymbol{\mu})\,|0\rangle = 0 \quad (3)$$

$$\langle\Phi_0|\,(1+\hat{\Lambda})(\bar{\hat{H}}(\boldsymbol{\lambda},\boldsymbol{\mu}) - \Delta E_{CC})\hat{q}_\rho\,|\Phi_0\rangle = 0, \quad \rho = 1, 2, \ldots \quad (4)$$

where $\hat{Q}$ is the projector operator $\hat{Q} = \sum_{m\neq 0} |\Phi_m\rangle\langle\Phi_m|$ and $\hat{q}_\rho = \{\hat{a}^\dagger \hat{i} \hat{b}^\dagger \hat{j} \ldots\}$, $\rho = 1, 2, \ldots$

First-order and second-order properties with respect to the strength parameters are obtained from the first and the second derivatives of $\Delta E_{CC}(\boldsymbol{\lambda},\boldsymbol{\mu})$ with respect to those parameters in the limit of zero strength: $\partial\Delta E_{CC}(\boldsymbol{\lambda},\boldsymbol{\mu})/\partial\lambda_i|_{\boldsymbol{\lambda},\boldsymbol{\mu}=0}$ (or $\partial\Delta E_{CC}(\boldsymbol{\lambda},\boldsymbol{\mu})/\partial\mu_i|_{\boldsymbol{\lambda},\boldsymbol{\mu}=0}$) and $\partial^2\Delta E_{CC}/\partial\lambda_i\partial\mu_j|_{\boldsymbol{\lambda},\boldsymbol{\mu}=0}$. Differentiation of $\Delta E_{CC}(\boldsymbol{\lambda},\boldsymbol{\mu})$in Equation (2) renders

$$\left.\frac{\partial\Delta E_{CC}(\boldsymbol{\lambda},\boldsymbol{\mu})}{\partial\lambda_i}\right|_{\boldsymbol{\lambda}=0} = \langle\Phi_0|\,(1+\hat{\Lambda})\bar{\hat{H}}_i^{(\lambda)}\,|\Phi_0\rangle + \sum_{j=1}^{N_\mu} \mu_j\,\langle\Phi_0|\,(1+\hat{\Lambda})\bar{\hat{H}}_{ij}^{(\lambda\mu)}\,|\Phi_0\rangle \quad (5)$$

$$\left.\frac{\partial^2\Delta E_{CC}(\boldsymbol{\lambda},\boldsymbol{\mu})}{\partial\lambda_i\partial\mu_j}\right|_{\boldsymbol{\lambda},\boldsymbol{\mu}=0} = \langle\Phi_0|\,\hat{\Lambda}^{\mu_i}\bar{\hat{H}}_i^{(\lambda)}\,|\Phi_0\rangle + \langle\Phi_0|\,(1+\hat{\Lambda})\big[\bar{\hat{H}}_i^{(\lambda)}, \hat{T}^{\mu_i}\big]\,|\Phi_0\rangle + \langle\Phi_0|\,(1+\hat{\Lambda})\bar{\hat{H}}_i^{(\lambda\mu)}\,|\Phi_0\rangle \quad (6)$$

where $\bar{\hat{H}}_i^{(\boldsymbol{\lambda})} = \exp(-\hat{T})\hat{H}_i^{(\boldsymbol{\lambda})}\exp(+\hat{T})$, $\bar{\hat{H}}_i^{(\boldsymbol{\lambda}\boldsymbol{\mu})} = \exp(-\hat{T})\hat{H}_i^{(\boldsymbol{\lambda}\boldsymbol{\mu})}\exp(+\hat{T})$, and $\hat{T}^{\mu_i}$ and $\hat{\Lambda}^{\mu_i}$ are the operator derivatives (or perturbed operators): $\hat{T}^{\mu_i}(\boldsymbol{\lambda},\boldsymbol{\mu}) = \partial\hat{T}(\boldsymbol{\lambda},\boldsymbol{\mu})/\partial\mu_i$ and $\hat{\Lambda}^{\mu_i}(\boldsymbol{\lambda},\boldsymbol{\mu}) = \partial\hat{\Lambda}(\boldsymbol{\lambda},\boldsymbol{\mu})/\partial\mu_i$. The relatively simple expression for $\partial\Delta E_{\mathrm{CC}}(\boldsymbol{\lambda},\boldsymbol{\mu})/\partial\lambda_i|_{\boldsymbol{\lambda},\boldsymbol{\mu}=0}$ in Equation (5) clearly manifests the effect of the generalised Hellmann–Feynman theorem [67] satisfied by $\Delta E_{\mathrm{CC}}(\boldsymbol{\lambda},\boldsymbol{\mu})$. The operator derivatives $\hat{T}^{\mu_i}$ and $\hat{\Lambda}^{\mu_i}$ are obtained by differentiating the $\hat{T}$- and $\hat{\Lambda}$-equations, Equations (3) and (4), respectively, with respect to the strength parameters [65]. As those equations show, the derivative operators $\hat{\Lambda}^{\mu_i}$ depend upon the $\hat{T}^{\mu_i}$ ones: $\hat{\Lambda}^{\mu_i} = \hat{\Lambda}^{\mu_i}(\hat{T}^{\mu_i})$ and are computationally more expensive than the last ones. However, the $\hat{\Lambda}^{\mu_i}$-equations can be combined with Equation (6) to eliminate the $\hat{\Lambda}^{\mu_i}$ from $\partial^2\Delta E_{\mathrm{CC}}(\boldsymbol{\lambda},\mu)/\partial\lambda_i\partial\mu_j|_{\boldsymbol{\lambda},\boldsymbol{\mu}=0}$ and express the latter exclusively in terms of $\hat{T}^{\lambda_i}$ and $\hat{T}^{\mu_i}$ [70]:

$$\begin{aligned}\left.\frac{\partial^2\Delta E_{\mathrm{CC}}\left(\boldsymbol{\lambda},\boldsymbol{\mu}\right)}{\partial\lambda_i\partial\mu_j}\right|_{\boldsymbol{\lambda},\boldsymbol{\mu}=0} &= \langle\Phi_0|\,(1+\hat{\Lambda})\big[\bar{\hat{H}}_i^{(\boldsymbol{\mu})},\hat{T}^{\lambda_i}\big]\,|\Phi_0\rangle\\ &+\langle\Phi_0|\,(1+\hat{\Lambda})\big[\bar{\hat{H}}_i^{(\boldsymbol{\lambda})},\hat{T}^{\mu_j}\big]\,|\Phi_0\rangle\\ &+\langle\Phi_0|\,(1+\hat{\Lambda})\big[\big[\bar{\hat{H}}\left(\boldsymbol{\lambda},\boldsymbol{\mu}\right),\hat{T}^{\mu_j}\big],\hat{T}^{\lambda_i}\big]\,|\Phi_0\rangle\\ &+\langle\Phi_0|\,(1+\hat{\Lambda})\bar{\hat{H}}_i^{(\boldsymbol{\lambda}\boldsymbol{\mu})}\,|\Phi_0\rangle\,. \end{aligned} \tag{7}$$

Equation (6) is termed the asymmetric $\partial^2\Delta E_{\mathrm{CC}}(\boldsymbol{\lambda},\mu)/\partial\lambda_i\partial\mu_j|_{\boldsymbol{\lambda},\boldsymbol{\mu}=0}$ expression with respect to the operator derivative variables because it requires the μ_i-derivatives $\hat{T}^{\mu_i}$ and $\hat{\Lambda}^{\mu_i}$ but not the λ_i-derivatives $\hat{T}^{\lambda_i}$ and $\hat{\Lambda}^{\lambda_i}$. In contrast, Equation (7) is termed the symmetric $\partial^2\Delta E_{\mathrm{CC}}(\boldsymbol{\lambda},\mu)/\partial\lambda_i\partial\mu_j|_{\boldsymbol{\lambda},\boldsymbol{\mu}=0}$ expression because it requires both μ_i- and λ_i-derivatives, more specifically, the $\hat{T}^{\lambda_i}$ and $\hat{T}^{\mu_i}$ but not the $\hat{\Lambda}^{\lambda_i}$ and $\hat{\Lambda}^{\mu_i}$. While Equations (6) and (7) are mathematically equivalent, Equation (7) is computationally less demanding than Equation (6) because the former does not require the operator derivatives $\hat{\Lambda}^{\mu_i}$. However, the asymmetry of Equation (6) can be exploited to increase its computational efficiency when the dimensions of the perturbations $\boldsymbol{\lambda}$ and $\boldsymbol{\mu}$, $N_{\boldsymbol{\lambda}}$ and $N_{\boldsymbol{\mu}}$, differ; in that case, the second perturbation $\boldsymbol{\mu}$ can be selected as the one having the smaller dimension $N_{\boldsymbol{\mu}}$ so that Equation (6) utilises the lowest possible number of operator derivatives $\hat{T}^{\mu_i}$ and $\hat{\Lambda}^{\mu_i}$. This situation is encountered in the calculation of NMR shielding [71], where $\boldsymbol{\lambda}$ and $\boldsymbol{\mu}$ can be conveniently chosen as the applied magnetic field $\mathbf{B}$ and the nuclear magnetic moments $\mathbf{F}_N$ by the N_N nuclei in a molecule, respectively, since $N_{\boldsymbol{\lambda}} = 3 < N_{\boldsymbol{\mu}} = 3N_N$ in all practical cases with $N_N \geq 2$. However, this computational saving cannot be applied to the calculation of static polarisabilities because in this case $\boldsymbol{\lambda} = \boldsymbol{\mu}$ = electric field $\mathbf{F}$ and $N_{\boldsymbol{\lambda}} = N_{\boldsymbol{\mu}} = 3$ [cf. Equation (8) below]. Currently, our general purpose LR-CC module employs the asymmetric Equation (6), while the symmetric Equation (7) will be implemented in the future.

For the static polarisabilities considered in this investigation, the perturbation part of $\hat{H}(\boldsymbol{\lambda},\boldsymbol{\mu})$ only contains a single first-order perturbation term:

$$\begin{aligned}\sum_{i=1}^{N_\lambda}\lambda_i\hat{H}_i^{(\boldsymbol{\lambda})} &= \sum_{i=1}^{3}F_i\hat{H}_i^{(\mathbf{F})};\quad i=1,2,3=x,y,z;\\ \hat{H}_i^{(\mathbf{F})} &= \sum_{p,q}h_{ipq}^{(\mathbf{F})}\left\{p^\dagger q\right\};\ h_{ipq}^{(\mathbf{F})}\\ &= -\langle p|-\sum_{n=1}^{N_e}r_{n_i}+\sum_{N=1}^{N_N}Z_NR_{N_i}\,|q\rangle \end{aligned} \tag{8}$$

where the strength parameter $\boldsymbol{\lambda}$ is an applied, static and uniform electric field $\mathbf{F} = (F_1,F_2,F_3)$, $\hat{H}_i^{(\boldsymbol{\lambda})} = \hat{H}_i^{(\mathbf{F})}$ is the component of the one-electron electric dipole operator, $h_{ipq}^{(\mathbf{F})}$ are the matrices elements of the one-electron part $\hat{H}_i^{(\mathbf{F})}$in the spin-orbital basis, $\mathbf{r}_n = (r_{n_1},r_{n_2},r_{n_3})$ and $\mathbf{R}_N = (R_{N_1},R_{N_2},R_{N_3})$ are the positions of the N_e electrons and N_N nuclei, respectively, and Z_N the nuclear charges. The first- and second-order properties corresponding to this perturbation term are the permanent dipole $\mathbf{p}_0$ and the polarisability tensor $\boldsymbol{\alpha}$, respectively. The latter is from Equations (6) and (8):

$$\begin{aligned}\alpha_{ij} = \left.\frac{\partial^2\Delta E_{\mathrm{CC}}}{\partial F_iF_j}\right|_{\mathbf{F}=\mathbf{0}} &= \langle\Phi_0|\,\hat{\Lambda}^{F_j}\bar{\hat{H}}_i^{(\mathbf{F})}\,|\Phi_0\rangle\\ &+\langle\Phi_0|\,(1+\hat{\Lambda})\big[\bar{\hat{H}}_i^{(\mathbf{F})},\hat{T}^{F_i}\big]\,|\Phi_0\rangle\\ &=\sum_{p,q}h_{ipq}^{(\mathbf{F})}\Delta D_{pq}^{(F_j)} \end{aligned} \tag{9}$$

where $\Delta D_{pq}^{(F_i)}$ are the elements of the correlated-corrected CC-response perturbed one-electron density matrix

$$\begin{aligned}\Delta D_{pq}^{(F_i)} &= \langle\Phi_0|\,\hat{\Lambda}^{F_i}\exp(-T)\left\{p^\dagger q\right\}\exp(+T)\,|\Phi_0\rangle\\ &+\langle\Phi_0|\,(1+\hat{\Lambda})[\exp(-T)\left\{p^\dagger q\right\}\exp(+T),\hat{T}^{F_i}] \end{aligned} \tag{10}$$

Expressions to evaluate other second-order properties (e.g. ESR $\mathbf{g}$- and $\mathbf{D}$-tensors) will be discussed in future publications [49].

3. Computational details, relevance of the investigated molecules and timing analysis

Static dipole polarisability tensors $\boldsymbol{\alpha}$ and some of their related properties [average static polarisabilities $\alpha_{\text{ave.}}$, static polarisability anisotropies $\Delta\alpha$ and perpendicular polarisabilities α_P, cf. Equation (11) and Section 4] are computed for 16 large molecules. To facilitate their study, these molecules are arranged into three sets according to their similarities in structure and chemical properties. Set I contains eight closed-shell molecules of interest in organic chemistry: quinoline, isoquinoline, benzonitrile, nitrobenzene, acenaphthene, benzanthracene, fluorene and thiophene (cf. Figure 1 for their structures). Set II contains the first four members of the closed-shell tiophene oligomer series: thiophene, 2,2′-bithiophene, 2,2′:5′,2″-terthiophene and 2,2′:5′,2″:5″,2‴-quaterthiophene (cf. Figure 1 for their structures). Finally, Set III contains five open-shell radicals: 1-3 pentadieneyl radical, C_5H_7 (doublet), 1-3-5-7 nonatetraeneyl radical, C_9H_{11} (doublet), 1-3-5 hexatriene cation radical, $C_6H_8{}^+$ (doublet), 1-3-5-7-9 decapentiene cation radical, $C_{10}H_{12}{}^+$ (doublet) and p-p-quinodimethane diradical, $C_8H_8 = \bullet CH_2 - C_6H_4 - CH_2\bullet$ (triplet). Thiophene is the only molecule included in two sets (Sets I and II) as explained in the next paragraph. Finally, a 17th closed-shell molecule: hexacene, $C_{26}H_{16}$, not included in any of the above sets, is employed in a polarisability calculation to generate timing data of the present massively parallel LR-CC module (cf. the discussion at the end of this section).

The molecules investigated herein are in principle selected because of their large sizes in order to demonstrate the capabilities of the present parallel implementation. Furthermore, in the case of the molecules in Sets I and II, the availability of experimental average polarisabilities $\alpha_{\text{ave.}}$ from various measurement techniques permits to ascertain the accuracy of both calculated and measured $\alpha_{\text{ave.}}$ (cf. the discussions in Section 4). Nevertheless, on selecting these molecules, special attention is also paid to the practical relevance of their polarisabilities in chemistry, physics, materials science and pharmacology. For instance, in the case of Set I, quinoline and isoquinoline are important in pharmacology, and understanding their electronic distributions in terms of their $\alpha_{\text{ave.}}$ is helpful to characterise their bacteriological activities [72]. Knowledge of the static polarisability tensor $\boldsymbol{\alpha}$ helps to explain the mesogenic properties of benzonitrile [73]. Nitrobenzene is used in Kerr cells due to its large Kerr constant [50]; the potential use of this material and others in Kerr cells based on their Kerr constants can be theoretically predicted from their static polarisability tensors $\boldsymbol{\alpha}$ [50]. The electroluminescence properties of fluorene can be explained from their electron distributions in terms of its $\alpha_{\text{ave.}}$ [74]. Calculations on the closed-shell molecules in

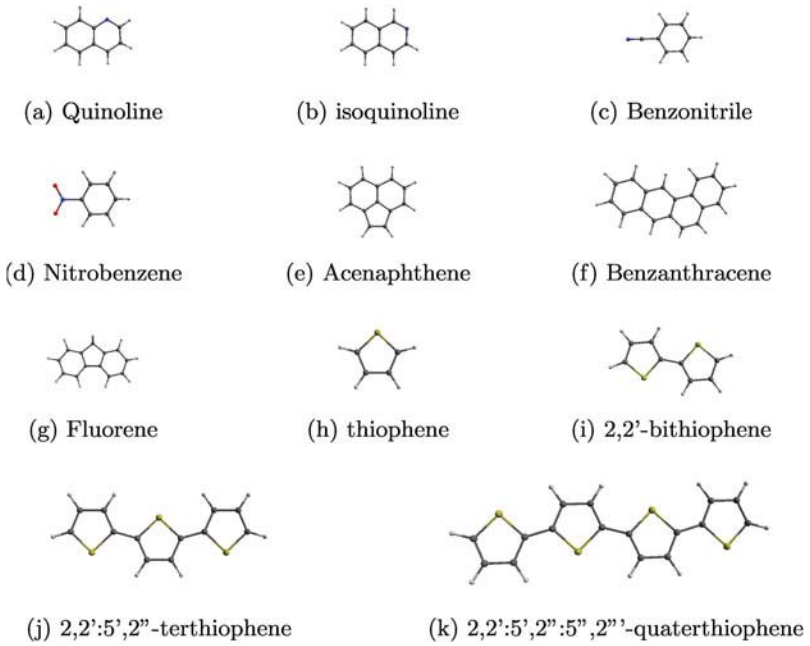

Figure 1. Structures of the 11 large molecules studied in this investigation. Set I of molecules: quinoline, isoquinoline, benzonitrile, nitrobenzene, acenaphthene, benzanthracene, fluorene and thiophene. Set II of molecules: thiophene and its successive oligomers: 2,2′-bithiophene, 2,2′:5′,2″-terthiophene and 2,2′:5′,2″:5″,2‴-quaterthiophene.

Set II permit the analysis of the variation of the thiophene oligomers' $\alpha_{\text{ave.}}(N)$ as a function of their number of thiophene units (monomers) N along the lines of previous studies of polymers' polarisabilities [9–11]. This type of analysis is important to predict conductive and optical properties of thiophene oligomers and polymers and helps to settle down the discrepancies between calculated and measured $\alpha_{\text{ave.}}(N)$ of these oligomers [56,75] (cf. Section 4). Finally, calculations on the open-shell radicals in Set III provide polarisability data so far unavailable experimentally due to the difficulties that these unstable radicals pose to their experimental determination [76,77]. Knowledge of accurate polarisabilities of these open-shell radicals is important for the hypothetical design of multifunction components that can change their conductive and optical properties upon change of their spin states by an external magnetic field [76,77].

For the closed-shell molecules in Sets I and II, static dipole polarisability tensors $\boldsymbol{\alpha}$ and related properties are calculated at the CPHF, MBPT(2) and CCSD levels to demonstrate the capabilities of the massively parallel LR-CC module in ACES III [41] and to examine the effect of increasing levels of electron correlation on the accuracy of the results. In addition, the same properties are calculated at the KS DFT level in order to compare the accuracies of wavefunction-based and DFT results. Present DFT calculations for $\boldsymbol{\alpha}$ are performed with the Perdew–Burke–Ernzerhof (PBE) functional [78] and its long-range-corrected (LC) [79] version, the LC-PBE functional; the latter displays a correct asymptotic behaviour in its exchange-correlation potential. For the open-shell molecules in Set III, static dipole polarisability tensors $\boldsymbol{\alpha}$ and related properties are calculated at the unrestricted CCSD (UCCSD) level. All the molecular geometries are calculated at the DFT/B3LYP [80] /6-311++G(2d,2p) level. Except in two cases discussed shortly, all the static dipole polarisability tensors $\boldsymbol{\alpha}$ are calculated with the Sadlej PVTZ basis sets [81], which, following Hammond *et al.* [82], produce results comparable to those obtained with the larger Dunning cc-PVTZ basis sets [83]. The two exceptions involve benzanthracene and 2,2′:5′,2″:5″,2‴-quaterthiophene. For these two molecules, Sadlej PVTZ basis sets show linear dependencies and, therefore, both Dunning cc-PVDZ and cc-PVTZ basis sets [83] are used instead. A comparison of the cc-PVDZ and cc-PVTZ results can gauge the convergence rate of these standard basis sets in polarisability calculations. All the present DFT and CPHF calculations are performed with the NWChem [38] code, while all the present MBPT(2), CCSD and UCCSD calculations are performed with the ACES III [71] code with our currently implemented LR-CC module.

Before discussing the present applications in the next section, it is opportune to discuss herein relevant timing data of the new massively parallel LR-CC module. These timing data are based on the polarisability calculation of hexacene, $C_{26}H_{16}$, an aromatic oligoacene with six benzene rings, at the CCSD level with the Dunning cc-PVTZ basis sets [83]; this calculation involves a total of 444 basis set functions. Table 1 lists the wall-clock times in minutes for all the LR-CC submodules involved in the aforesaid calculation: the HF calculation and partial post-HF transformation, the CCSD $\hat{T}$- and $\hat{\Lambda}$-equations, Equations (3) and (4), the CCSD $\hat{T}^{\mu_i}(\boldsymbol{\lambda}, \boldsymbol{\mu})$ and $\hat{\Lambda}^{\mu_i}(\boldsymbol{\lambda}, \boldsymbol{\mu})$ derivative calculations, and the CCSD density $\Delta D_{pq}^{(F_i)}$ calculation, Equation (10), and final assembly. Times for the CCSD $\hat{T}$- and $\hat{\Lambda}$-equations submodules and for the CCSD $\hat{T}^{\mu_i}(\boldsymbol{\lambda}, \boldsymbol{\mu})$ and $\hat{\Lambda}^{\mu_i}(\boldsymbol{\lambda}, \boldsymbol{\mu})$ derivatives submodules are per iteration; these procedures experience on average 14, 14, 29 and 27 iterations, respectively. Timing data are presented as a function of the number of utilised computer cores: 400, 800 and 1600 cores. These timings are not generated on dedicated nodes and as a result the absolute times do not reflect too

Table 1. Timing data of the present massively parallel LR-CC module for the case of the polarisability calculation of hexacene, $C_{26}H_{16}$, at the CCSD level with the Dunning cc-PVTZ basis sets [83] (= a total of 444 basis set functions). Wall-clock times per each LR-CC submodule are reported in minutes as a function of the number of computer cores. Times for the CCSD $\hat{T}$- and $\hat{\Lambda}$-equations procedures and the CCSD $\hat{T}^{\mu_i}(\boldsymbol{\lambda}, \boldsymbol{\mu})$ and $\hat{\Lambda}^{\mu_i}(\boldsymbol{\lambda}, \boldsymbol{\mu})$ derivatives calculations are per iteration; these procedures experience on average 14, 14, 29 and 27 iterations, respectively.

LR-CC submodule	Wall-clock times with 400 cores	Wall-clock times with 800 cores	Wall-clock times with 1600 cores
HF calculation and partial post-HF transformation	7	12	12
CCSD $\hat{T}$-equation calculation	4	3	2
CCSD $\hat{\Lambda}$-equation calculation	6	4	2
CCSD $\hat{T}^{\mu_i}(\boldsymbol{\lambda}, \boldsymbol{\mu})$ derivatives calculation	13	12	10
CCSD $\hat{\Lambda}^{\mu_i}(\boldsymbol{\lambda}, \boldsymbol{\mu})$ derivatives calculation	9	6	3
CCSD density $\Delta D_{pq}^{(F_i)}$ calculation and final assembly	13	8	4

well the performance of the individual submodules. The meaningful data to examine is how the present submodules perform as the number of cores increases. It can be seen from Table 1 that all our CCSD submodules after the HF one scale very well in the range of the considered processors. The utilised 444-function basis set is not large enough to reveal any significant scaling in the HF calculation and partial post-HF transformation. In fact, their performance gets degraded, but this is not unusual for these tasks. One of the issues to be addressed in the future is the non-ideal rate of convergence of the CCSD $\hat{T}^{\mu_i}(\boldsymbol{\lambda}, \boldsymbol{\mu})$ and $\hat{\Lambda}^{\mu_i}(\boldsymbol{\lambda}, \boldsymbol{\mu})$ derivatives submodules.

4. Results and discussion

4.1. Calculated and experimental polarisabilities

In this study, we calculate the nine-component static dipole polarisability tensor $\boldsymbol{\alpha}$ and its related properties: the average (scalar) static polarisabilities $\alpha_{\text{ave.}}$ and the static polarisability anisotropies $\Delta\alpha$ [50]:

$$\begin{aligned}\alpha_{\text{ave.}} &= \left|\frac{1}{3}\text{Tr}\,(\boldsymbol{\alpha})\right| = \left|\frac{1}{3}\left(\alpha_{xx}+\alpha_{yy}+\alpha_{zz}\right)\right|;\\ \Delta\alpha &= +\sqrt{\frac{1}{2}\left[3\text{Tr}\,(\boldsymbol{\alpha}^2) - Tr^2\,(\boldsymbol{\alpha})\right]}\\ &= +\sqrt{\frac{1}{2}\left[\left(\alpha'_{xx}-\alpha'_{yy}\right)^2+\left(\alpha'_{xx}-\alpha'_{zz}\right)^2+\left(\alpha'_{yy}-\alpha'_{zz}\right)^2\right]}\end{aligned} \tag{11}$$

where $\boldsymbol{\alpha}' = (\delta_{ij}\alpha'_{ij})$ is the diagonalised static dipole polarisability tensor $\boldsymbol{\alpha}$. There are various experimentally determined $\alpha_{\text{ave.}}$ for the molecules in Sets I and II to ascertain the accuracy of the calculated $\alpha_{\text{ave.}}$ (cf. Tables 2–4). However, there are no experimentally determined $\Delta\alpha$ to compare with their calculated counterparts. Therefore, the calculated $\Delta\alpha$ are of a predictive nature. In addition, the calculated $\Delta\alpha$ provide an extra variable to compare the employed theoretical methods among themselves. For the molecules in Sets I and II, we only report their calculated $\alpha_{\text{ave.}}$ and $\Delta\alpha$. For the molecules in Set III, we report these same properties as well as the components α_{ij} of their tensors $\boldsymbol{\alpha}$ and their perpendicular polarisabilities $\alpha_P = |\alpha_{ii}|$ (cf. Section 4.3 for further details); while no experimental polarisability data are available for the molecules in Set III, some previously calculated α_P are available for comparison [76].

Since comparisons between theoretical and experimental $\alpha_{\text{ave.}}$ are important, it is instructive to analyse the available experimentally determined $\alpha_{\text{ave.}}$ and their accuracy. All the experimental average static polarisabilities $\alpha_{\text{ave.}}(\omega = 0)$ employed in this study were determined from average dynamic polarisabilities $\alpha_{\text{ave.}}(\omega \neq 0)$ measured with refractometric techniques on liquid samples at or near room temperature. The refractometric techniques measure the refractive index $n(\omega)$ of the liquid samples employing light with a frequency $\omega \neq 0$; from the $n(\omega)$, average dynamic polarisabilities $\alpha_{\text{ave.}}(\omega \neq 0)$ are calculated via the Lorentz–Lorenz relationship [50]: $\alpha_{\text{ave}}(\omega) = (3/4\pi\rho)\ \{[n(\omega)^2 - 1]\ /\ [n(\omega)^2 + 2]\}$, where ρ is the number density (i.e. the number of particles per unit volume) of a gas or liquid sample. To determine the average static $\alpha_{\text{ave.}}(\omega = 0)$, several dynamic $\alpha_{\text{ave.}}(\omega \neq 0)$ are determined at different frequencies $\omega \neq 0$ and fitted into the Cauchy dispersion equation [50]: $\alpha_{\text{ave.}}(\omega) = \alpha_{\text{ave.}}(\omega = 0) + C_2\omega^2 + C_4\omega^4 + \cdots$, where $C_2, C_4, \ldots$ etc. are the Cauchy coefficients, from which $\alpha_{\text{ave.}}(\omega = 0)$ can be immediately determined. However, in the case of thiophene and its oligomers (Set II), only their dynamic $\alpha_{\text{ave}}(\omega)$ in tetrahydrofuran solution measured with a single light wavelength $\lambda = 2\pi c/\omega = 589$ nm are available [75]. For these molecules, the static

Table 2. Average static dipole polarisabilities $\alpha_{\text{ave.}}$, Equation (11), in atomic units of the closed-shell molecules in Sets I and II from CPHF, DFT-PBE, DFT-LC-PBE, MBPT(2) and CCSD calculations and from experiments. All calculations are performed with the Sadlej PVTZ basis sets [81] except where otherwise indicated. Additional experimental data are listed in Tables 3 and 4.

Molecule	CPHF	DFT-PBE	DFT-LC-PBE	MBPT(2)	CCSD	Experiments
Quinoline	110.3	116.7	112.14	113.1	113.6	118.2 [87], cf. Table 3
Isoquinoline	109.4	115.6	111.3	112.7	112.6	112.9 [87], cf. Table 3
Benzonitrile	83.6	88.4	85.1	83.1	85.0	84.4 [73], cf. Table 4
Nitrobenzene	83.6	89.7	86.0	84.2	87.1	99.2 [88]
Acenaphthene	138.9	145.0	139.2	144.2	141.0	139.0. [74]
Benzanthracene	226.8	247.0	231.1	213.8	201.6[a]218.2[b]	218.0
Fluorene	148.2	159.0	150.8	147.4	152.4	146.4.[74]
Thiophene	62.5	65.3	63.2	64.6	64.5	55.9 [56,75]
2,2′-bithiophene	132.10	143.0	134.0	137.7	135.5	124.2 [56,75]
2,2′:5′,2"-terthiophene	216.4	246.2	219.9	207.0	219.6	195.8 [56,75]
2,2′:5′,2":5",2"′-quaterthiophene	312.4	375.7	317.3	266.2	265.53[a]290.6[b]	377.7 [56,75]

[a]Dunning cc-PVDZ basis set [83].
[b]Dunning cc-PVTZ basis set [83].

Table 3. Measured average static dipole polarisabilities $\alpha_{\text{ave.}}$, Equation (11), in atomic units of quinolone and isoquinoline from various experimental sources.

Quinoline	Isoquinoline
105.8[a]	105.4[a]
111.8[b]	111.3[b]
112.0[c]	110.9[c]
118.2 [d,*]	112.9 [d,*]
105.1[d]	113.2[d]
106.4[d]	119.5[d]
111.9[d]	112.7[d]
109.3[d]	117.2[d]
113.4[e]	117.1 [e]
114.7[e]	118.4[e]

[a]Ref. [89].
[b]Ref. [74].
[c]Ref. [90].
[d]Ref. [87].
[e]Ref. [88].
*Selected for Table 2.

$\alpha_{\text{ave.}}(\omega \neq 0)$ were determined through a relationship proposed by Champagne *et al.* [56]: $\alpha(\omega) = \alpha(\omega = 0)(\Delta E^2 - \hbar^2\omega^2)/\Delta E^2$, where ΔE is the experimental excitation energies from the ground to the first-excited states of the molecules [75]. This two-state relationship is obviously approximate because it neglects contributions of higher excited states, but a better estimation of $\alpha(\omega = 0)$ is not possible with the available data. The refractometric techniques were applied to liquid samples of the molecules under study. In one measurement for benzonitrile, a neat (i.e. pure liquid) sample was utilised [73]. However, the rest of the refractometric measurements involved solutions of the molecules in relatively inert solvents. In those cases, the determinations of the dynamic $\alpha_{\text{ave.}}(\omega)$ involved the use of solvent models (e.g. Lorentz [84,85] and Onsager [86] local fields) to account for solute–solvent interactions. In conclusion, it follows from the above considerations that the experimentally determined static $\alpha_{\text{ave.}}$ should be considered with care because of the various manipulations and assumptions during their determinations. On the other hand, the calculated average static $\alpha_{\text{ave.}}$ are for single non-interacting molecules in gas phase at 0 K. One should bear in mind all these assumptions in the experimental and calculated data during their comparisons.

4.2. Polarisabilities of closed-shell molecules and thiophene oligomers (Sets I and II)

Table 2 lists the average dipole polarisabilities $\alpha_{\text{ave.}}$ of the closed-shell molecules in Sets I and II calculated at the CPHF, DFT-PBE, DFT-LC-PBE, MBPT(2) and CCSD levels with the basis sets discussed in Section 3. In addition, Table 2 lists the experimentally determined $\alpha_{\text{ave.}}$ of these selected molecules from different experimental sources. In the cases of quinoline, isoquinoline and benzonitrile, various experimentally determined $\alpha_{\text{ave.}}$ are available for each molecule, and all those values are listed in Tables 3 (quinoline and isoquinoline) and 4 (benzonitrile). For quinoline and isoquinoline, all their experimentally determined $\alpha_{\text{ave.}}$ are from measurements in solution; therefore, their most recently measured $\alpha_{\text{ave.}}$ [87] in cyclohexane are taken as their most reliable experimental values for comparison in Table 2. For benzonitrile, its experimental $\alpha_{\text{ave.}}$ are from one neat measurement [73] and from various measurements [73] in solution; therefore, the $\alpha_{\text{ave.}}$ from the neat sample is taken as its most reliable experimental value for comparison in Table 2. Analysis of the data in Table 2 reveals that the average absolute error $|\alpha_{\text{ave}}^{\text{Calc.}} - \alpha_{\text{ave}}^{\text{Expt.}}|$ of the calculated average polarisabilities, $\alpha_{\text{ave}}^{\text{Calc.}}$, with respect to the experimental ones, $\alpha_{\text{ave}}^{\text{Expt.}}$, for the molecules in Set I is: 5.9 (CPHF), 9.8 (DFT-PBE), 6.3 (DFT-LC-PBE), 5.2 [MBPT(2)] and 4.5 a.u. (CCSD), respectively. Similarly, the average absolute error $|\alpha_{\text{ave}}^{\text{Calc.}} - \alpha_{\text{ave}}^{\text{Expt.}}|$ for the molecules in Set II is: 25.1 (CPHF), 20.1 (DFT-PBE), 25.4 (DFT-LC-PBE), 36.2 [MBPT(2)] and 32.7 a.u. (CCSD), respectively. Finally, the average absolute error $|\alpha_{\text{ave}}^{\text{Calc.}} - \alpha_{\text{ave}}^{\text{Expt.}}|$ for all the molecules in Sets I and II is: 12.8 (CPHF), 13.6 (DFT-PBE), 13.1 (DFT-LC-PBE), 16.2 [MBPT(2)] and 14.6 a.u. (CCSD), respectively. On calculating the above errors, the experimental $\alpha_{\text{ave}}^{\text{Expt.}}$ are taken from Table 2 and the CCSD $\alpha_{\text{ave}}^{\text{Calc.}}$ of benzanthracene

Table 4. Measured average static dipole polarisabilities $\alpha_{\text{ave.}}$, Equation (11), in atomic units of benzonitrile from various experimental sources.

Solvent		Lorentz local field [84,85]	Onsager local field [86]
Neat (pure liquid) [73]	80.6*		
CCl_4 [73]		81.5	81.5
C6H12 [73]		83.7	83.68
THF [73]		84.5	83.9
CH_3CN [73]		83.0	82.3

*Selected for Table 2.

and 2,2′:5′,2″:5″,2‴-quaterthiophene are those calculated with the cc-PVTZ basis sets. As a reference, it is worth noticing that the standard deviations of the experimental $\alpha_{ave}^{Expt.}$ in Tables 3 and 4 are: 4.0 (quinolone), 4.0 (isoquinoline) and 1.2 (benzonitrile) a.u., respectively, while the reported error bar in the determination of $\alpha_{ave}^{Expt.}$ for benzonitrile is approximately 5 a.u. [73].

Overall, the calculated $\alpha_{ave}^{Calc.}$ for the molecules in Set I show a satisfactory agreement with the available experimental results in Tables 2–4. Comparison of the CPHF $\alpha_{ave}^{Calc.}$ with their experimental counterparts shows that, unlike the case of ESR isotropic hyperfine coupling constants [48], electron correlation effects are not excessively critical for the accuracy of the calculated $\alpha_{ave}^{Calc.}$ in Set I since the CPHF $\alpha_{ave}^{Calc.}$ agree reasonably well with the experimental data. Therefore, it is understandable that all the calculated $\alpha_{ave}^{Calc.}$ with the employed wavefunction-based and DFT correlated methods in Set I agree well with the experimental data. With the exception of acenaphthene and thiophene, addition of correlation effects to the CPHF $\alpha_{ave}^{Calc.}$ in the simplest wavefunction-based form via MBPT(2) improves the accuracy of the calculated $\alpha_{ave}^{Calc.}$ in Set I. A better overall agreement with the experimental data in Set I is finally achieved with the highly correlated CCSD $\alpha_{ave}^{Calc.}$, although for isoquinoline, benzonitrile and fluorene, the MBPT(2) $\alpha_{ave.}$ agree slightly better with the experimental $\alpha_{ave.}^{Expt.}$ than the CCSD $\alpha_{ave}^{Calc.}$ do. In the case of the DFT calculations for Set I, DFT-PBE overall performs worse than CPHF, whereas DFT-LC-PBE overall performs better than DFT-PBE but still worse than CPHF; these DFT performances may be attributed to the deterioration of the exchange interaction in DFT-PBE with respect to that in HF and to the partial restoration of the correct HF exchange interaction in DFT-PBE-LC through its ad hoc partition of the operator r_{12}^{-1} into short- and long-range components [79]. Despite observed differences, all the employed theoretical methods perform consistently well in predicting the $\alpha_{ave.}$ of the molecules in Set I.

As mentioned previously, Set II permits one to analyse the variation of the thiophene oligomers' $\alpha_{ave.}(N)$ as a function of their number of thiophene units (monomers) N along the lines of previous studies of polymers' polarisabilities [9–11]. More specifically, an early study by Champagne *et al.* [56] provided the $\alpha_{ave.}(N)$ of these oligomers for $N = 1 - 7$ at the sum-over-states (SOS) and CPHF levels. Plots of the SOS and CPHF increments $\alpha_{ave.}(N+1) - \alpha_{ave.}(N)$ of these oligomers vs. N become nearly constant at about $N = 3 - 6$ [56] – a phenomenon termed saturation that is expected from chemical intuition. In other words, the SOS and CPHF $\alpha_{ave.}(N)$ reach a nearly linear dependency upon N very early at about $N = 3 - 6$. In contrast, the experimentally

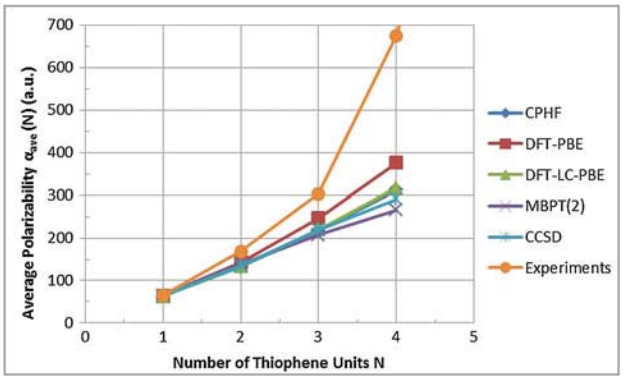

Figure 2. Total average static polarisabilities $\alpha_{ave.}(N)$ of the thiophene oligomers as a function of the thiophene units N from CPHF, DFT-PBE, DFT-LC-PBE, MBPT(2) and CCSD calculations and from experiments [56,75].

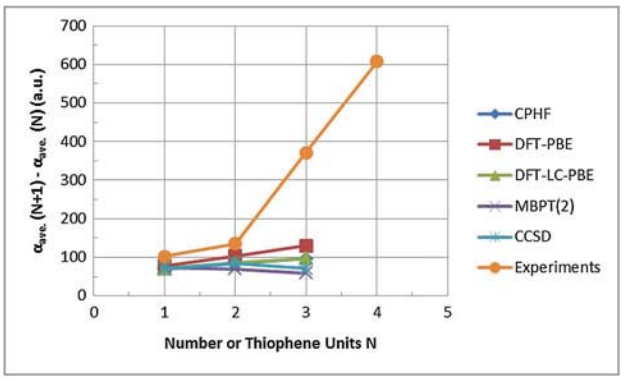

Figure 3. Increments of the total average static polarisabilities $\alpha_{ave.}(N+1) - \alpha_{ave.}(N)$ of the thiophene oligomers as a function of the thiophene units N from CPHF, DFT-PBE, DFT-LC-PBE, MBPT(2) and CCSD calculations and from experiments [56,75].

determined increments $\alpha_{ave.}(N+1) - \alpha_{ave.}(N)$ do not show any sign of saturation even with their highest available oligomer at $N + 1 = 6$ [60,75] but a monotonically increasing and steep pattern. Thus, there was a great discrepancy between the calculated and experimental $\alpha_{ave.}(N)$ but the lack of calculated $\alpha_{ave.}(N)$ with high-level methods and of additional experimental $\alpha_{ave.}(N)$ at that time prevented from determining which data were incorrect: either the calculated or the experimental ones. Fortunately, the present parallel implementation of high-level methods can help to resolve this controversy. Toward that goal, Figure 2 shows plots of $\alpha_{ave.}(N)$ vs. N for the first four thiophene oligomers from the current CPHP, DFT-PBE, DFT-LC-PBE, MBPT(2) and CCSD calculations and from experiments [60,75]; in addition, Figure 3 shows plots of $\alpha_{ave.}(N+1) - \alpha_{ave.}(N)$ vs. N from the first four thiophene oligomers for the same type of data in Figure 2. In agreement with the calculated $\alpha_{ave.}(N)$ by Champagne *et al.* [56], all the currently calculated $\alpha_{ave.}(N)$ for the thiophene oligomers display a saturation

Table 5. Static dipole polarisability anisotropies $\Delta\alpha$, Equation (11), in atomic units for the closed-shell molecules in Sets I and II from CPHF, DFT-PBE, DFT-LC-PB, MBPT(2) and CCSD calculations. All calculations are performed with the Sadlej PVTZ basis sets [81] except where otherwise indicated.

Molecule	CPHF	PBE	LC-PBE	MBPT(2)	CCSD
Quinoline	81.3	92.3	85.7	66.9	85.2
Isoquinoline	77.1	88.2	82.1	64.9	81.3
Benzonitrile	56.9	66.4	61.0	44.7	58.4
Nitrobenzene	52.2	63.3	57.1	42.9	56.1
Acenaphthene	98.3	108.0	101.7	86.0	100.6
Benzanthracene	218.0	261.1	229.7	165.5	185.5[a]
Fluorene	109.6	130.8	116.7	75.6	114.9
Thiophene	28.3	31.6	30.2	26.1	30.1
2,2′-bithiophene	94.7	117.1	99.9	66.7	96.1
2,2′:5′,2"-terthiophene	206.9	282.8	217.2	115.3	204.2
2,2′:5′,2":5",2"′-quaterthiophene	360.1	532.7	374.2	185.9	355.2[a]

[a]Dunning cc-PVTZ basis set [83].

pattern at low values of N. It may be safe to conclude now that all the discussed theoretical methods must be correct in predicting this early saturation, while the experimental $\alpha_{\text{ave.}}(N)$ appear inaccurate. Given the provenance of experimental $\alpha_{\text{ave.}}$ as discussed in Section 4.1, it is not possible to indicate the source(s) of the possible inaccuracy in the experimental $\alpha_{\text{ave.}}(N)$ of the thiophene oligomers. Only further theoretical and experimental studies of these systems will shed light on the remaining questions. In agreement with the trends found with the molecules in Set I, the CPHF, DFT-PBE-LC, MBPT(2) and CCSD $\alpha_{\text{ave.}}(N)$ of the thiophene oligomers in Set II are relatively close in values, but the DFT-PBE $\alpha_{\text{ave.}}(N)$ appear somewhat higher in value in comparison with the other theoretical results (cf. Figure 2). The behaviour of the DFT-PBE $\alpha_{\text{ave.}}(N)$ vs. N is consistent with previous observations of DFT overestimation of $\alpha_{\text{ave.}}$ in polymers with common DFT functionals [9–11]. In this case, the observed DFT-PBE overestimation may be attributed again to the inaccurate description of the exchange interaction by the PBE functional since the corrected DFT-LC-PBE $\alpha_{\text{ave.}}(N)$ does not manifest this overestimation within the available interval of N values. Oddly, DFT-PBE exhibits the lowest absolute error in Set II. This apparent accuracy is obviously not significant due to the fact that it is an artefact of the unphysical DFT-PBE overestimation (cf. Figure 2) and due to the uncertainty in the experimental $\alpha_{\text{ave.}}(N)$.

Table 5 lists the static polarisability anisotropies $\Delta\alpha$, Equation (11), of the closed-shell molecules in Sets I and II calculated at the CPHF, DFT-PBE, DFT-LC-PBE, MBPT(2) and CCSD levels with the basis sets discussed in Section 3. The $\Delta\alpha$ in Table 5 are also displayed as a bar plot in Figure 4. Analysis of the calculated $\Delta\alpha$ in Table 5 and Figure 4 reveals that CPHF, DFT-LC-PBE and CCSD predict comparable $\Delta\alpha$, whereas DFT-PBE and MBPT(2) over- and underestimate the $\Delta\alpha$, respectively, in comparison with the other results. The DFT-PBE

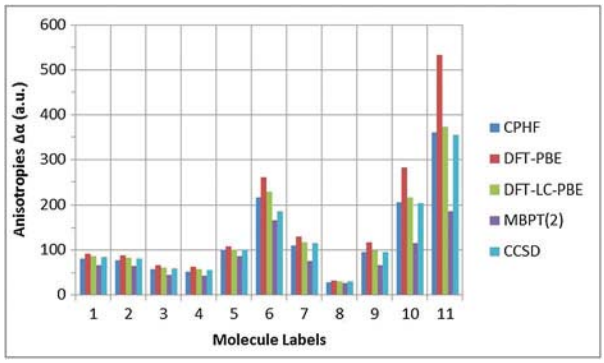

Figure 4. Polarisability anisotropies $\Delta\alpha$, Equation (11), in atomic units from CPHF, DFT-PBE, DFT-LC-PBE, MBPT(2) and CCSD calculations for the 11 considered molecules labelled as: 1: quinoline, 2: isoquinoline, 3: benzonitrile, 4: nitrobenzene, 5: acenaphthene, 6: benzanthracene, 7: fluorene, 8: thiophene, 9: 2,2′-bithiophene, 10: 2,2′:5′,2′′-terthiophene and 11: 2,2′:5′,2′′:5′′,2′′′-quaterthiophene.

overestimation of $\Delta\alpha$ may be correlated with its overestimation of $\alpha_{\text{ave.}}$. The MBPT(2) underestimation of $\Delta\alpha$ is somewhat unexpected, especially when the MBPT(2) and CCSD $\alpha_{\text{ave.}}$ behave as expected. Obviously, this discrepancy between CCSD and MBPT(2) $\Delta\alpha$ must be reflected in the magnitude of the diagonal elements of the $\boldsymbol{\alpha}$ tensor (cf. Equation (11)). To illustrate this, let us inspect the MBPT(2) and CCSD diagonal tensor elements of quinoline: a molecule that shows the largest difference between the two anisotropy values in Set I. They are $\alpha'_{xx} = 116.4974$, $\alpha'_{yy} = 161.1931$, $\alpha'_{zz} = 61.01207$ a.u. for CCSD and $\alpha'_{xx} = 118.4822$, $\alpha'_{yy} = 148.8335$, $\alpha'_{zz} = 72.1012$ a.u. for MBPT(2), respectively. As we can clearly see, the differences in the distribution of the magnitude of the diagonal elements in the tensor directions are responsible for the anomalous behaviour of the compared CCSD and MBPT(2) $\Delta\alpha$, while the average polarisability $\alpha_{\text{ave.}}$ remains in agreement. This is an interesting observation but provides no obvious explanation for

Table 6. Components of the static polarisability tensor $\boldsymbol{\alpha} = (\alpha_{ij})(i, j = x, y, z)$ with respect to the principal axes of inertia, average static dipole polarisabilities $\alpha_{\text{ave.}}$ and polarisability anisotropies $\Delta\alpha$, Equation (11), in atomic units for the radicals in Set III from current UCCSD calculations with Sadlej PVTZ basis sets [81]. Also listed are the perpendicular polarisabilities $\alpha_P = |\alpha_{ii}|$ at the current UCCSD level (first entry) in comparison with available theoretical values [76] (second entry) at the UCCSD(T) or RO-MBPT(2) level with Dunning cc-PVDZ basis sets [83] or modified Dunning cc-PVDZ basis sets [76] for all the radicals except C_8H_8.

Radical	Properties		
C_5H_7	Polarisability tensor components $\alpha_{ij}(i, j = x, y, z)$		
	$\alpha_{XX} =$ -119.4	$\alpha_{XY} = 0.0$	$\alpha_{XZ} = 0.0$
	$\alpha_{YX} = 0.0$	$\alpha_{YY} = -44.5$	$\alpha_{YZ} = 0.0$
	$\alpha_{ZX} = 0.0$	$\alpha_{ZY} = 0.0$	$\alpha_{ZZ} = -56.8$
	Average polarisability $\alpha_{\text{ave.}} = 73.6$		
	Polarisability anisotropy $\Delta\alpha = 69.5$		
	Perpendicular polarisability $\alpha_P = \lvert\alpha_{XX}\rvert = 119.4$		
	(current UCCSD/Sadlej PVTZ);110.0 [UCCD(T)/modified cc-PVDZ [76]]		
C_9H_{11}	Polarisability tensor components $\alpha_{ij}(i, j = x, y, z)$		
	$\alpha_{XX} = -95.7$	$\alpha_{XY} = -0.2$	$\alpha_{XZ} = 0.0$
	$\alpha_{YX} = -0.2$	$\alpha_{YY} = -310.5$	$\alpha_{YZ} = 0.0$
	$\alpha_{ZX} = 0.0$	$\alpha_{ZY} = 0.0$	$\alpha_{ZZ} = -72.5$
	Average polarisability $\alpha_{\text{ave.}} = 159.6$		
	Polarisability anisotropy $\Delta\alpha = 227.3$		
	Perpendicular polarisability $\alpha_P = \lvert\alpha_{YY}\rvert = 310.5$ (current UCCSD/Sadlej PVTZ);		
	$= 350.7$ [RO-MBPT(2)/modified cc-PVDZ [76]]		
$C_6H_8^+$	Polarisability tensor components $\alpha_{ij}(i, j = x, y, z)$		
	$\alpha_{XX} = -59.2$	$\alpha_{XY} = 4.4$	$\alpha_{XZ} = 0.0$
	$\alpha_{YX} = 4.4$	$\alpha_{YY} = -213.7$	$\alpha_{YZ} = 0.0$
	$\alpha_{ZX} = 0.0$	$\alpha_{ZY} = 0.0$	$\alpha_{ZZ} = -41.3$
	Average polarisability $\alpha_{\text{ave.}} = 104.7$		
	Polarisability anisotropy $\Delta\alpha = 164.4$		
	Perpendicular polarisability $\alpha_P = \lvert\alpha_{YY}\rvert = 213.7$ (current UCCSD/Sadlej PVTZ);		
	$= 200.0$ [UCCSD(T)/cc-PVDZ [76]]		
$C_{10}H_{12}^+$	Polarisability tensor components $\alpha_{ij}(i, j = x, y, z)$		
	$\alpha_{XX} = -98.8$	$\alpha_{XY} = -14.1$	$\alpha_{XZ} = 0.0$
	$\alpha_{YX} = -14.0$	$\alpha_{YY} = -629.2$	$\alpha_{YZ} = 0.0$
	$\alpha_{ZX} = 0.0$	$\alpha_{ZY} = 0.0$	$\alpha_{ZZ} = -69.3$
	Average polarisability $\alpha_{\text{ave.}} = 265.8$		
	Polarisability anisotropy $\Delta\alpha = 546.3$		
	Perpendicular polarisability $\alpha_P = \lvert\alpha_{YY}\rvert = 629.2$ (current UCCSD/Sadlej PVTZ);		
	$= 549.0$ [UCCSD(T)/cc-PVDZ [76]]		
C_8H_8	Polarisability tensor components $\alpha_{ij}(i, j = x, y, z)$		
	$\alpha_{XX} = -59.1$	$\alpha_{XY} = 0.0$	$\alpha_{XZ} = 0.0$
	$\alpha_{YX} = 0.0$	$\alpha_{YY} = -181.2$	$\alpha_{YZ} = 0.0$
	$\alpha_{ZX} = 0.0$	$\alpha_{ZY} = 0.0$	$\alpha_{ZZ} = -86.9$
	Average polarisability $\alpha_{\text{ave.}} = 109.1$		
	Polarisability anisotropy $\Delta\alpha = 110.9$		
	Perpendicular polarisability $\alpha_P = \lvert\alpha_{YY}\rvert = 181.2$ (current UCCSD/Sadlej PVTZ)		

this behaviour, which will be further investigated in the future.

4.3. Polarisability of the open-shell radicals (Set III)

Table 6 lists the components of the static dipole polarisability tensors $\boldsymbol{\alpha} = (\alpha_{ij})$ $i, j = x, y, z$ with respect to the principal axes of inertia, the average static polarisabilities $\alpha_{\text{ave.}}$, the static polarisability anisotropies $\Delta\alpha$ and the perpendicular polarisabilities $\alpha_P = |\alpha_{ii}|$ of the open-shell radicals in Set III at the UCCSD level with the Sadlej PVTZ basis sets [81]. Also listed in Table 6 are previously calculated α_P [76] at the restricted-open-shell MBPT(2) [RO-MBPT(2)] (C_9H_{11}) and unrestricted CCSD(T) [UCCSD(T)] levels (C_5H_7, $C_6H_8^+$ and $C_{10}H_{12}^+$) with the Dunning cc-PVDZ [83] (C_5H_7 and C_9H_{11}) and modified Dunning cc-PVDZ basis sets [76] ($C_6H_8^+$ and $C_{10}H_{12}^+$). No previously calculated α_P for the C_8H_8 biradical are available for comparison. For each molecule, the longitudinal, lateral and perpendicular polarisabilities are the absolute values of the diagonal elements of its polarisability tensors $\boldsymbol{\alpha}$, $|\alpha_{ii}|$, with respect to the three principal axes of inertia that are (nearly) along the molecule backbone, on the molecule plane/quasi-plane containing the previous axis, and perpendicular to the molecule plane/quasi-plane, respectively [76]. These three polarisabilities are important to understand the conductive and optical properties of materials; however, the perpendicular polarisability α_P is analysed in more detail because it is the only type of polarisability of these radicals for which previously calculated values are available for comparison [76]. The absolute deviations between the present and previous [76] α_P, $|\alpha_p^{\text{Present}} - \alpha_p^{\text{Previous}}|$, are 9.4 ($C_5H_7$), 40.2

(C_9H_{11}), 13.7 ($C_6H_8^+$) and 80.2 a.u. ($C_{10}H_{12}^+$), which are larger than the largest experimental error of 5 a.u. for the measurement of $\alpha_{ave.}$ in benzonitrile [73] considered in this study. In addition, the percentage relative deviation between the present and previous [76] α_P, $|\alpha_p^{Present} - \alpha_p^{Previous}| \times 100/\alpha_P^{Ref.}$, where the reference polarisability $\alpha_P^{Ref.}$ is that calculated with the more correlated method for a given radical [UCCSD for C_9H_{11} and UCCSD(T) for the rest] is 8.5 (C_5H_7), 13.0 (C_9H_{11}), 6.9 ($C_6H_8^+$) and 14.6% ($C_{10}H_{12}^+$). These deviations suggest that the calculated polarisabilities of these radicals are rather sensitive to the level of electronic correlation in the employed method and the size of the basis set. Consistently, previously calculated ESR isotropic hyperfine coupling constants of radicals [48] were similarly sensitive. Future calculations with various correlated methods and basis sets will shed further light on this issue. As stated previously, there are no experimental polarisabilities of these unstable radicals to date; therefore, the previous [76] and present calculated polarisabilities are truly predictive. We hope that all these predictive values will spur the interest to corroborate them with further calculations and experimental measurements.

5. Conclusions

As part of our ongoing implementation of parallel CC capabilities to evaluate ESR properties [48,49], we present herein a new massively parallel LR-CC module within the ACES III code [41] to calculate up to second-order properties. This module employs the cutting-edge parallel-computing tools in ACES III [41], such as the SIP [45] and the SIAL [46]. This general-purpose LR-CC module can be used to evaluate any type of first- and second-order properties of both closed- and open-shell molecules employing restricted, unrestricted and restricted-open-shell HF references. Due to the relevance of static polarisabilities in various applied sciences, we illustrate this LR-CC module through the calculation of that second-order property in large molecules at the MBPT(2) (closed-shell cases) and CCSD (closed- and open-shell cases) levels. In addition, closed-shell calculations at the CPHF and DFT levels are included for comparison. This study focuses on 16 large molecules sorted into three sets. Set I includes eight closed-shell molecules relevant in organic chemistry: quinoline, isoquinoline, benzonitrile, nitrobenzene, acenaphthene, benzanthracene, fluorene and thiophene. Set II includes the closed-shell oligomer series: thiophene, 2,2′-bithiophene, 2,2′:5′,2″-terthiophene and 2,2′:5′,2″:5″,2‴-quaterthiophene; the polarisabilities of these molecules are relevant to elucidate conductive and optical properties in thiophene polymers. Finally, Set III includes five open-shell radicals: 1-3 pentadieneyl radical, C_5H_7, 1-3-5-7 nonatetraeneyl radical, C_9H_{11}, 1-3-5 hexatriene cation radical, $C_6H_8^+$, 1-3-5-7-9 decapentiene cation radical, $C_{10}H_{12}^+$, and p-p-quinodimethane diradical, C_8H_8; the polarisabilities of these radicals are relevant for designing multifunction components that can change their conductive and optical properties upon change of their spin states by an external magnetic field [76,77]. All calculations are performed with the Sadlej PVTZ basis sets [81], except for the CCSD calculations of benzanthracene and 2,2′:5′,2″:5″,2‴-quaterthiophene that are performed with the Dunning cc-PVDZ and cc-PVTZ basis sets [83]. The calculated polarisabilities of the closed-shell molecules in Sets I and II are compared with various experimental polarisabilities, whose determinations from measurements and accuracies are examined in detail. No experimental data are available for the radicals in Set III and the calculated data are, therefore, truly predictive. For Set I, all the calculated average static polarisabilities agree reasonably well with the experimental data, with DFT-PBE and CCSD providing the worst and best agreements, respectively. This indicates that, unlike ESR properties in open-shell radicals [48], electron correlation effects are less critical for the accuracy of polarisabilities in closed-shell molecules. For Set II, the calculated average static polarisabilities vs. the number of monomer units exhibit comparable values and saturation patterns with all the employed methods, in agreement with earlier low-level calculations [56]. In Set II, the disagreement of all these calculated data with the experimental ones [75] suggests inaccuracies in the latter. In Sets I and II, DFT-PBE tends to somewhat overestimate the average static polarisability, a phenomenon previously observed with some DFT functionals [9–11]. Calculated static polarisability anisotropies in Sets I and II show comparable values among all the employed methods, except for MBPT(2), which predicts relatively low values. For Set III, UCCSD perpendicular static polarisabilities show a reasonable agreement with their counterparts previously calculated at the UCCSD(T) and RO-MBPT(2) levels [76]. Like ESR properties in open-shell radicals [48], the calculated polarisabilities of these open-shell radicals are somewhat sensitive to the level of electron correlation effects in the employed methods. Timing data of this LR-CC module are exemplified with additional CCSD polarisability calculations on hexacene, $C_{26}H_{16}$.

Acknowledgments

The authors are indebted to Mr Austin Privett (graduate student at Texas Tech University: TTU) for his assistance to prepare the figures for this manuscript. All the present calculations have been performed at the TTU High Performance Computer

Center (TTU HPCC), The University of Florida High Performance Computer Center (HyperGator), the TTU Chemistry Computer Cluster (TTU CCC), and the Texas Advanced Computing Cluster (TACC) at the University of Texas at Austin. The authors thank the TTU HPCC and TACC for providing free computer time to run some of the present calculations.

Disclosure statement

No potential conflict of interest was reported by the authors.

Funding

The American Chemical Society Petroleum Research Fund [grant number PRF#51773-ND6].

References

[1] T. Helgaker, S. Coriani, P. Jørgensen, K. Kristensen, J. Olsen, and K. Ruud, Chem. Rev. (Washington, DC, US) **112**, 543 (2012).
[2] R.J. Bartlett and M. Musiał, Rev. Mod. Phys. **79**, 291 (2007).
[3] F. Neese, Coord. Chem. Rev. **253**, 526 (2009).
[4] J. Leszczynski and M. Shukla, *Practical Aspects of Computational Chemistry I: An Overview of the Last Two Decades and Current Trends* (Springer, Berlin, 2012).
[5] J. Leszczynski and M. Shukla, *Practical Aspects of Computational Chemistry II: An Overview of the Last Two Decades and Current Trends* (Springer, Berlin, 2012).
[6] P. Hohenberg and W. Kohn, Phys. Rev. **136**, B864 (1964).
[7] W. Kohn and L.J. Sham, Phys. Rev. **140**, A1133 (1965).
[8] W. Koch and M.C. Holthausen, *A Chemist's Guide to Density Functional Theory*, 2nd ed. (Wiley-VCH, New York, 2001).
[9] S.J.A. van Gisbergen, P.R.T. Schipper, O.V. Gritsenko, E.J. Baerends, J.G. Snijders, B. Champagne, and B. Kirtman, Phys. Rev. Lett. **83**, 694 (1999).
[10] B. Kirtman, S. Bonness, A. Ramirez-Solis, B. Chanpagne, H. Matsumoto, and H. Sekino, J. Chem. Phys. **128**, 114108 (2008).
[11] S. Nenon, B. Champagne, and M.I. Spassova, Phys. Chem. Chem. Phys. **16**, 7083 (2014).
[12] J.P. Perdew and A. Ruzsinszky, Int. J. Quantum Chem. **110**, 2801 (2010).
[13] J.P. Perdew, A. Ruzsinszky, L.A. Constantin, J. Sun, and G.I. Csonka, J. Chem. Theory Comput. **5**, 902 (2009).
[14] A.J. Cohen, P. Mori-Sanchez, and W. Yang, J. Chem. Phys. **129**, 121104 (2008).
[15] P. Verma, A. Perera, and R.J. Bartlett, Chem. Phys. Lett. **524**, 10 (2012).
[16] P. Verma and R.J. Bartlett, J. Chem. Phys. **137**, 134102 (2012).
[17] A. Ruzsinszky, J.P. Perdew, G.I. Csonka, O.A. Vydrov, and G.E. Scuseria, J. Chem. Phys. **126**, 104102 (2007).
[18] M. Lundberg and P.E.M. Siegbahn, J. Chem. Phys. **122**, 224103 (2005).
[19] O.A. Vydrov and G.E. Scuseria, J. Chem. Phys. **125**, 234109 (2006).
[20] A.J. Cohen, P. Mori-Sánchez, and W. Yang, Science **321**, 792 (2008).
[21] R. McWeeny, *Methods of Molecular Quantum Mechanics*, 2nd ed. (Academic Press, London, 1992).
[22] I. Shavitt and R.J. Bartlett, *Many-Body Methods in Chemistry and Physics: MBPT and Coupled-Cluster Theory* (Cambridge University Press, New York, NY, 2009).
[23] R.J. Bartlett, Mol. Phys. **108**, 2905 (2010).
[24] P. Carsky, J. Paldus, and J. Pittner, *Recent Progress in Coupled Cluster Methods: Theory and Applications, Challenges and Advances in Computational Chemistry and Physics* (Springer, Berlin, 2010).
[25] R J. Bartlett and D.M. Silver, Int. J. Quantum Chem. **9**, 183 (1975).
[26] K.A. Brueckner, Phys. Rev. **97**, 1353 (1955).
[27] A.G. Taube, PhD dissertation, University of Florida, Department of Chemistry, Gainesville, FL, 2008.
[28] A.G. Taube and R.J. Bartlett, J. Chem. Phys. **130**, 144112 (2009).
[29] K. Raghavachari, G.W. Trucks, J.A. Pople, and M. Head-Gordon, Chem. Phys. Lett. **157**, 479 (1989).
[30] R.J. Bartlett, J.D. Watts, S.A. Kucharski, and J. Noga, Chem. Phys. Lett. **165**, 513 (1990).
[31] J.F. Stanton, J. Gauss, M.E. Harding, and P.G. Szalay, CFOUR, Coupled Cluster Techniques for Computational Chemistry, a quantum-chemical program package (1992–2010).
[32] M.S. Gordon and M.W. Schmidt, in *Theory and Applications of Computational Chemistry*, edited by C.E. Dykstra, G. Frenking, K.S. Kim, and G.E. Scuseria (Elsevier, Amsterdam, 2005), pp. 1167–1189.
[33] J.L. Bentz, R.M. Olson, M.S. Gordon, M.W. Schmidt, and R.A. Kendall, Comput. Phys. Commun. **176**, 589 (2007).
[34] R.M. Olson, J.L. Bentz, R.A. Kendall, M.W. Schmidt, and M.S. Gordon, J. Comput. Theor. Chem. **3**, 1312 (2007).
[35] M.J. Frisch, G.W. Trucks, H.B. Schlegel, G.E. Scuseria, M.A. Robb, J.R. Cheeseman, G. Scalmani, V. Barone, B. Mennucci, G.A. Petersson, H. Nakatsuji, M. Caricato, X. Li, H.P. Hratchian, A.F. Izmaylov, J. Bloino, G. Zheng, J.L. Sonnenberg, M. Hada, M. Ehara, K. Toyota, R. Fukuda, J. Hasegawa, M. Ishida, T. Nakajima, Y. Honda, O. Kitao, H. Nakai, T. Vreven, J.A. Montgomery, Jr., J.E. Peralta, F. Ogliaro, M. Bearpark, J.J. Heyd, E. Brothers, K.N. Kudin, V.N. Staroverov, R. Kobayashi, J. Normand, K. Raghavachari, A. Rendell, J.C. Burant, S.S. Iyengar, J. Tomasi, M. Cossi, N. Rega, J.M. Millam, M. Klene, J.E. Knox, J.B. Cross, V. Bakken, C. Adamo, J. Jaramillo, R. Gomperts, R.E. Stratmann, O. Yazyev, A.J. Austin, R. Cammi, C. Pomelli, J.W. Ochterski, R.L. Martin, K. Morokuma, V.G. Zakrzewski, G.A. Voth, P. Salvador, J.J. Dannenberg, S. Dapprich, A.D. Daniels, Ö. Farkas, J.B. Foresman, J.V. Ortiz, J. Cioslowski, and D.J. Fox, *Gaussian 09, Revision D.01* (Gaussian, Inc., Wallingford, CT 2009).
[36] H.-J. Werner, P.J. Knowles, G. Knizia, F.R. Manby, M. Schütz, P. Celani, T. Korona, R. Lindh, A. Mitrushenkov, G. Rauhut, K.R. Shamasundar, T.B. Adler, R.D. Amos, A. Bernhardsson, A. Berning, D.L. Cooper, M.J.O. Deegan, A.J. Dobbyn, E. Goll, C. Hampel, A. Hesselmann, G. Hetzer, T. Hrenar, G. Jansen, C. Köppl, Y. Liu, A.W. Lloyd, R.A. Mata, A.J. May, S.J. McNicholas, W. Meyer,

M.E. Mura, A. Nicklass, D.P. O'Neill, P. Palmieri, D. Peng, K. Pflüger, R. Pitzer, M. Reiher, T. Shiozaki, H. Stoll, A.J. Stone, R. Tarroni, T. Thorsteinsson, and M. Wang, MOLPRO, version 2012.1, a package of ab initio programs (2012).

[37] H.-J. Werner, P.J. Knowles, G. Knizia, F.R. Manby, and M. Schütz, WIREs Comput. Mole. Sci. **2**, 242 (2012).

[38] M. Valiev, E.J. Bylaska, N. Govind, K. Kowalski, T.P. Straatsma, H.J.J. Van Dam, D. Wang, J. Nieplocha, E. Apra, T.L. Windus, and W.A. de Jong, Comput. Phys. Commun. **181**, 1477 (2010).

[39] F. Neese, Comput. Mol. Sci. **2**, 73 (2012).

[40] Y. Shao, Z. Gan, E. Epifanovsky, A.T.B. Gilbert, M. Wormit, J. Kussmann, A.W. Lange, A. Behn, J. Deng, X. Feng, D. Ghosh, M. Goldey, P.R. Horn, L.D. Jacobson, I. Kaliman, R.Z. Khaliullin, T. Kus, A. Landau, J. Liu, E.I. Proynov, Y.M. Rhee, R.M. Richard, M.A. Rohrdanz, R.P. Steele, E.J. Sundstrom, H.L. Woodcock, P.M. Zimmerman, D. Zuev, B. Albrecht, E. Alguire, B. Austin, G.J.O. Beran, Y.A. Bernard, E. Berquist, K. Brandhorst, K.B. Bravaya, S.T. Brown, D. Casanova, C. Chang, Y. Chen, S.H. Chien, K.D. Closser, D.L. Crittenden, M. Diedenhofen, R.A. DiStasio, H. Do, A.D. Dutoi, R.G. Edgar, S. Fatehi, L. Fusti-Molnar, A. Ghysels, A. Golubeva-Zadorozhnaya, J. Gomes, M.W.D. Hanson-Heine, P.H.P. Harbach, A.W. Hauser, E.G. Hohenstein, Z.C. Holden, T. Jagau, H. Ji, B. Kaduk, K. Khistyaev, J. Kim, J. Kim, R.A. King, P. Klunzinger, D. Kosenkov, T. Kowalczyk, C.M. Krauter, K.U. Lao, A.D. Laurent, K.V. Lawler, S.V. Levchenko, C.Y. Lin, F. Liu, E. Livshits, R.C. Lochan, A. Luenser, P. Manohar, S.F. Manzer, S. Mao, N. Mardirossian, A.V. Marenich, S.A. Maurer, N.J. Mayhall, E. Neuscamman, C.M. Oana, R. Olivares-Amaya, D.P. O'Neill, J.A. Parkhill, T.M. Perrine, R. Peverati, A. Prociuk, D.R. Rehn, E. Rosta, N.J. Russ, S.M. Sharada, S. Sharma, D.W. Small, A. Sodt, T. Stein, D. Stueck, Y. Su, A.J.W. Thom, T. Tsuchimochi, V. Vanovschi, L. Vogt, O. Vydrov, T. Wang, M.A. Watson, J. Wenzel, A. White, C.F. Williams, J. Yang, S. Yeganeh, S.R. Yost, Z. You, I.Y. Zhang, X. Zhang, Y. Zhao, B.R. Brooks, G.K.L. Chan, D.M. Chipman, C.J. Cramer, W.A. Goddard, M.S. Gordon, W.J. Hehre, A. Klamt, H.F. Schaefer, M.W. Schmidt, C.D. Sherrill, D.G. Truhlar, A. Warshel, X. Xu, A. Aspuru-Guzik, R. Baer, A.T. Bell, N.A. Besley, J. Chai, A. Dreuw, B.D. Dunietz, T.R. Furlani, S.R. Gwaltney, C. Hsu, Y. Jung, J. Kong, D.S. Lambrecht, W. Liang, C. Ochsenfeld, V.A. Rassolov, L.V. Slipchenko, J.E. Subotnik, T. van Voorhis, J.M. Herbert, A.I. Krylov, P.M.W. Gill, and M. Head-Gordon, Mol. Phys. **113**, 184 (2015).

[41] V. Lotrich, N. Flocke, M. Ponton, A.D. Yau, A. Perera, E. Deumens, and R.J. Bartlett, J. Chem. Phys. **128**, 194104 (2008).

[42] J. Baker, K. Wolinski, M. Malagoli, D. Kinghorn, P. Wolinski, G. Magyarfalvi, S. Saebo, T. Janowski, and P. Pulay, J. Comput. Chem. **30**, 317 (2009).

[43] J.R. Hammond, K. Kowalski, and W.A. De Jong, J. Chem. Phys. **127**, 144105 (2007).

[44] K. Kowalski, J.R. Hammond, W.A. De Jong, and A.J. Sadlej, J. Chem. Phys. **129**, 226101 (2008).

[45] V.F. Lotrich, J.M. Ponton, A.S. Perera, E. Deumens, R.J. Bartlett, and B.A. Sanders, Mol. Phys. **108**, 3323 (2010).

[46] E. Deumens, V.F. Lotrich, A. Perera, M.J. Ponton, B.A. Sanders, and R.J. Bartlett, Wiley Interdisciplinary Rev. Comput. Mol. Sci. **1**, 895 (2011).

[47] N. Flocke and V. Lotrich, J. Comput. Chem. **29**, 2722 (2008).

[48] P. Verma, S.A. Perera, and J.A. Morales, J. Chem. Phys. **139**, 174103 (2013).

[49] P. Verma, A. Perera, and J.A. Morales, J. Chem. Phys. (2015) (in preparation).

[50] K.D. Bonin and V.V. Kresin, *Electric-Dipole Polarizabilities of Atoms, Molecules, and Clusters* (World Scientific, Singapore, 1997).

[51] G. Maroulis, *Computational Aspects of Electric Polarizability Calculations: Atoms, Molecules and Clusters* (IOS Press, Amsterdam, 2006).

[52] R.G. Parr and W. Yang, *Density-Functional Theory of Atoms and Molecules, The International Series of Monographs on Chemistry* (Oxford University Press, New York, 1989).

[53] M.J. Packer, E.K. Dalskov, S.P.A. Sauer, and J. Oddershede, Theor. Chim. Acta **89**, 323 (1994).

[54] S.P.A. Sauer and J. Oddershede, Int. J. Quantum Chem. **50**, 317 (1994).

[55] E.K. Dalskov and S.P.A. Sauer, J. Phys. Chem. A **102**, 5269 (1998).

[56] B. Champagne, D.H. Mosley, and J.-M. Andre, J. Chem. Phys. **100**, 2034 (1993).

[57] M. Ferrero, M. Rerat, B. Kirtman, and R. Dovesi, J. Chem. Phys. **129**, 244110 (2008).

[58] B. Champagne and B. Kirtman, Int. J. Quantum Chem. **109**, 3103 (2009).

[59] J.F. Stanton and R.J. Bartlett, J. Chem. Phys. **99**, 5178 (1993).

[60] P.B. Rozyczko, A. Perera, M. Nooijen, and R.J. Bartlett, J. Chem. Phys. **107**, 6736 (1997).

[61] H.J. Monkhorst, Int. J. Quantum Chem. **S11**, 421 (1977).

[62] E. Dalgaard and H.J. Monkhorst, Phys. Rev. A **28**, 1217 (1983).

[63] H. Koch and P. Jorgensen, J. Chem. Phys. **93**, 3333 (1990).

[64] T.B. Pedersen and H. Koch, J. Chem. Phys. **106**, 8059 (1997).

[65] I. Shavitt and R.J. Bartlett, *Many-Body Methods in Chemistry and Physics: MBPT and Coupled-Cluster Theory, Cambridge Molecular Science* (Cambridge University Press, New York, 2009).

[66] J. Arponen, Ann. Phys. **151**, 311 (1983).

[67] E.A. Salter, G.W. Trucks, and R.J. Bartlett, J. Chem. Phys. **90**, 1752 (1989).

[68] G. Fitzgerald, R.J. Harrison, and R.J. Bartlett, J. Chem. Phys. **85**, 5143 (1986).

[69] L. Adamowicz, W.D. Laidig, and R.J. Bartlett, Int. J. Quantum Chem. **26**, 245 (1984).

[70] A. Perera, M. Nooijen, and R.J. Bartlett, J. Chem. Phys. **104**, 3290 (1996).

[71] J. Gauss, J. Chem. Phys. **99**, 3629 (1993).

[72] A. Hinchliffe and H.J. Soscun Machadao, J. Mol. Struct. (Theochem) **312**, 57 (1994).

[73] Y. Alvarado, P. Labarca, N. Cubilln, E. Osorio, and A. Karam, Zeitschrift fur Naturforschung A J. Phys. Sci. **58**, 68 (2003).

[74] J. Schuyer, L. Blom, and D.W. van Krevelen, Trans. Faraday Soc. **49**, 1391 (1953).

[75] M.T. Zhao, B.P. Singh, and P.N. Prasad, J. Chem. Phys. **89**, 5535 (1988).
[76] B. Champagne, E. Botek, O. Quinet, M. Nakano, R. Kishi, T. Nitta, and K. Yamaguchi, Chem. Phys. Lett. **407**, 372 (2005).
[77] R. Kishi, S. Bonness, K. Yoneda, H. Takahashi, M. Nakano, E. Botek, B. Champagne, T. Kubo, K. Kamada, K. Ohta, and T. Tsunesa, J. Chem. Phys. **132**, 094107 (2010).
[78] J.P. Perdew, K. Burke, and M. Ernzerhof, Phys. Rev. Lett. **77**, 3865 (1996).
[79] Y. Tawada, T. Tsuneda, S. Yanagisawa, T. Yanai, and K. Hirao, J. Chem. Phys. **120**, 8425 (2004).
[80] A.D. Becke, J. Chem. Phys. **98**, 5648 (1993).
[81] A.J. Sadlej, Czech. Chem. Commun. **53**, 1995 (1988).
[82] J.R. Hammond, N. Govind, K. Kowalski, J. Autschbach, and S.S. Xantheas, J. Chem. Phys. **131**, 214103 (2009).
[83] J.T.H. Dunning, J. Chem. Phys. **90**, 1007 (1989).
[84] L.T. Cheng, W. Tam, S. Stevenson, G. Meredith, G. Rikkne, and S. Marder, J. Chem. Phys. **95**, 10631 (1991).
[85] K. Singer and A. Garito, J. Chem. Phys. **75**, 3572 (1981).
[86] L. Onsanger, J. Am. Chem. Soc. **58**, 1486 (1936).
[87] Y. Alvarado, N. Cubilln, M. Leal, P. Labarca, E. Michelena, and Y. Marrero Ponce, J. Solution Chem. **36**, 1139 (2007).
[88] K.J. Miller, J. Am. Chem. Soc. **112**, 8533 (1990).
[89] C.G. Le Fèvre, R.J.W. Le Fèvre, B. Purnachandra Rao, and A.J. Williams, J. Chem. Soc. **123**, (1960). http://pubs.rsc.org/en/Content/ArticleLanding/1960/JR/JR9600000123#!divAbstract
[90] S. Batsanov, *Refractometry and Chemical Structure* (Consultants Bureau, New York, 1961).